Am J Cancer Res 2023;13(10):4623-4643
www.ajcr.us /ISSN:2156-6976/ajcr0152095

Original Article

The modulation of local and systemic anti-tumor immune response induced by methotrexate nanoconjugate in murine MC38 colon carcinoma and B16 F0 melanoma tumor models

Agnieszka Szczygieł, Katarzyna Węgierek-Ciura, Jagoda Mierzejewska, Anna Wróblewska, Joanna Rossowska, Natalia Anger-Góra, Bożena Szermer-Olearnik, Marta Świtalska, Tomasz M Goszczyński, Elżbieta Pajtasz-Piasecka

Hirszfeld Institute of Immunology and Experimental Therapy, Polish Academy of Sciences, Wrocław, Poland

Received July 7, 2023; Accepted September 15, 2023; Epub October 15, 2023; Published October 30, 2023

Abstract: Methotrexate (MTX) which is one of the longest-used cytostatics, belongs to the group of antimetabolites and is used for treatment in different types of cancer as well as during autoimmune diseases. MTX can act as a modulator enable to create the optimal environment to generate the specific anti-tumor immune response. A novel system for MTX delivery is its conjugation with high-molecular-weight carriers such as hydroxyethyl starch (HES), a modified amylopectin-based polymer applied in medicine as a colloidal plasma volume expander. Such modification prolongs the plasma half-life of the HES-MTX nanoconjugate and improves the distribution of the drug in the body. In the current study, we focused on evaluating the dose-dependent therapeutic efficacy of chemotherapy with HES-MTX nanoconjugate compared to the free form of MTX, and examining the time-dependent changes in the local and systemic anti-tumor immune response induced by this therapy. To confirm the higher effectiveness of HES-MTX in comparison to MTX, we analyzed its action using murine MC38 colon carcinoma and B16 F0 melanoma tumor models. It was noted that HES-MTX at a dose of 20 mg/kg b.w. was more effective in tumor growth inhibition than MTX in both tumor models. One of the main differences between the two analyzed tumor models concerned the kinetics of the appearance of the immunomodulation. In MC38 tumors, the beneficial change in the tumor microenvironment (TME) landscape, manifested by the depletion of pro-tumor immune cells, and increased influx of cells with strong anti-tumor activity was noted already 3 days after HES-MTX administration, while in B16 F0 model, these changes occurred 10 days after the start of therapy. Thus, the immunomodulatory potential of the HES-MTX nanoconjugate may be closely related to the specific immune cell composition of the TME, which combined with additional treatment such as immunotherapies, would enhance the therapeutic potential of the nanoconjugate.

Keywords: Nanoconjugate, methotrexate, immune response, immunomodulation, chemotherapy, colon carcinoma, MC38, melanoma, B16

Introduction

Chemotherapeutics according to their mechanisms of action are categorized into seven pillars of anti-cancer therapy concerning 80 cytotoxic drugs available for the treatment of cancers [1]. The effect of chemotherapy is based not only on fighting cancer cells but also on activating the host's immune system, which contributes to effective elimination of the tumor. Cytostatics, especially administered in appropriate doses, reveal their immunomodulatory potential enabling the temporary depletion of immune cells with suppressor activity such as myeloid-derived suppressor cells (MDSCs), tumor-associated macrophages (TAMs), or regulatory T cells (Tregs), but may also increase the number of effector cells with cytotoxic properties in the tumor microenvironment (TME) [2-7]. Preclinical studies are mostly based on well-known chemotherapeutics, such as cyclophosphamide, paclitaxel, doxorubicin, or methotrexate [1]. Methotrexate (MTX) which is one of the longest-used cytostatic, belongs to the group of antimetabolites, responsible for the reduction of folates required for DNA syn-

thesis. It is used for the treatment of leukemias, lymphomas, osteosarcomas, breast, head and neck, bladder, and trophoblastic neoplasms as well as during autoimmune diseases, such as rheumatoid arthritis [8]. However, MTX likewise doxorubicin or cyclophosphamide, can act as a modulator enable to create the optimal cytokine environment to generate the specific anti-tumor immune response [9].

Methotrexate enters cells mainly via the ubiquitous reduced folate carrier (RFC) [10]. This pathway is also responsible for the systemic toxicity of this cytostatic [11, 12]. In some cases, the binding of cytostatic can be carried out by the α subunit of the folate receptor (FRα), but due to the low affinity of MTX molecule to this receptor, this pathway of entry does not play a major role in the antiproliferative activity of the cytostatic [12].

The main problems in anti-cancer therapy, associated with the use of low molecular weight compounds, such as MTX, are their rapid removal and adverse body distribution. To avoid the above problem, research is being conducted on the design of a selective drug delivery system that will allow targeted accumulation of the drug in the tumor tissue [13]. For this purpose, various MTX carriers have been used i.a. micelles [14], dendrimers [15, 16], or nanocapsules [17]. An example of a novel form of MTX delivery is the conjugation of this cytostatic to high molecular carriers such as hydroxyethyl starch (HES). This amylopectin-based modified polymer is applied in medicine as colloidal plasma volume expanders, and widely used as nanocarrier in targeted anti-cancer therapy [18-22]. The process of conjugating those molecules takes place directly by covalently linking hydroxyl groups of HES to carboxyl groups of MTX through an ester bond. The release of the cytostatic from the nanoconjugate occurs as a result of hydrolysis and enzymatic degradation by amylases, which leads to the degradation to glucose, maltose and methotrexate. Thus, through the covalent coupling of MTX and HES, nanoconjugate has a longer plasma half-time compared to the free form of MTX, and importantly - improved drug biodistribution in the body. Furthermore, the improvement of the specificity of the nanoconjugate interaction with cancer cells is based on its polyvalency, as a result of which approximately 50 MTX molecules can attach to one HES molecule [23]. Such modification is helpful for nanoconjugate to enter cells via folate receptors (FRs), including FRα present on cancer cells, instead of mention above ubiquitously expressed RFCs [12].

The hydrodynamic diameter (dH) of the HES-MTX molecule ranged 15.2 ± 6.2 nm [23]. There is evidence that nanoparticles with a hydrodynamic diameter above 10 nm, do not penetrate through the blood vessel wall into healthy tissues [24]. On the other hand, rapid angiogenesis which occurs especially in solid tumors leads to the formation of leaky blood vessels [25] accompanied by enhanced vascular permeability and retention effect (EPR). Thus, the nanoconjugate, opposite to healthy tissues, would be able to penetrate the tumor tissue and the extension of the half-life of the cytostatic attached to the carrier increases the chance of the drug reaching the tumor tissue [26]. This aspect was discussed in our previous publication [27]. Then, due to the prolonged accumulation of the HES-MTX in the tumor tissue, and increased affinity for FRα, we assumed its higher anticancer activity compared to MTX. In fact, the first therapeutic experiments using this nanoconjugate confirmed its superior therapeutic effect compared to MTX against both murine (P388) and human (MV4-11) leukemia tumors [23].

Although MTX is used in anticancer therapy, there are few reports evaluating its effect on immune cells. Therefore, we attempt to answer the question of whether the attachment of MTX to a carrier ensuring better drug distribution will result in beneficial changes in the local and systemic anti-tumor immune response. Moreover, by evaluating the modulation of immune response occurring over time and through detailed characteristics of various immune cell subpopulations involved in the creation of this response, it will be possible to define when and which cells were the most affected by the use of HES-MTX nanoconjugate and determine how this may be related with a delay of tumor growth.

Materials and methods

Mice

Female C57BL/6 mice were obtained from the Center of Experimental Medicine of the Medical

University of Białystok (Białystok, Poland). Mice were kept in a room with a standard light/dark cycle, with a constant temperature (22 ± 2°C), air humidity (55 ± 10%), and access to food and water *ad libitum*. All experiments were performed in accordance with EU Directive 2010/63/EU for animal experiments and were approved by the Local Ethics Committee for Experiments with the use of Laboratory Animals, Wrocław, Poland (authorization No. 077/2019 and 009/2021). After experiments, mice were sacrificed by cervical dislocation.

Cell culture

The *in vivo* growing MC38 murine colon carcinoma from the Tumor Bank of the Radiobiological Institute TNO (Rijswijk, The Netherlands) was adapted to *in vitro* conditions as described by Pajtasz-Piasecka [28]. The culture of MC38/0 (named here MC38) cells was maintained in RPMI-1640 (Gibco; Thermo Fisher Scientific, Inc.) supplemented with 100 U/ml penicillin, 100 mg/ml streptomycin, 0.5% sodium pyruvate, 0.05 mM 2-mercaptoethanol (named here RPMI) and 5% fetal bovine serum (FBS; all reagents from Sigma-Aldrich; Merck KGaA). The culture of non-metastatic murine melanoma B16 F0 cell line (ECACC 92101204) was maintained in Dulbecco's Modified Eagle Medium (ATCC) high-glucose supplemented with 100 U/ml penicillin, 100 mg/ml streptomycin and 10% FBS (Sigma-Aldrich; Merck KGaA). All cell cultures were grown at 37°C, 95% humidity and 5% CO_2.

Therapeutic treatment schedule

Eight-to-ten-week-old female C57BL/6 mice were subcutaneously (s.c.) inoculated in the right flank with MC38 cells (1.1×10^6 cells/0.2 ml NaCl 0.9%/mouse) or B16 F0 cells (3.0×10^4 cells/0.1 ml MariGel/mouse). When tumor nodules were palpable, mice were randomly divided based on tumor volume into seven experimental groups. The therapeutic schedule started from intravenously (i.v.) injection in the tail vein of chemotherapeutics - MTX (Ebewe Pharma) or HES-MTX nanoconjugate (HES-MTX preparation was described in [23, 27]) in doses 5, 20 or 40 mg/kg of body weight. During the experiments, two or three times a week, tumors were measured by using an electronic caliper and tumor volume was calculated according to the formula: $a/2\times b^2$, where a represents the largest and b represents the smallest tumor diameter [29]. The therapeutic efficacy was determined based on the tumor growth inhibition (TGI) value calculated as follows: TGI (%) = 100 - ($TV_t/TV_{nt}\times100$), where TV_t refers to a median tumor volume in the treated group and TV_{nt} - median tumor volume in the non-treated (nt) group [30]. The health of the mice was constantly monitored (weight loss, bristling hair, lethargy) and when the tumor volume was >2 cm^3 the mice were sacrificed. In order to estimate the impact of applied chemotherapy on local and systemic anti-tumor immune response, 3 and 10 days after administration of MTX-based chemotherapeutics, spleen and tumor nodules were dissected from tumor bearing mice (from 3-7 mice per group), homogenized and stored in liquid nitrogen for further *ex vivo* analyses.

Analysis of myeloid and lymphoid cell populations in MC38 or B16 F0 tumors after applied therapy

Single cell suspensions of tumor tissue were thawed and stained for identification of myeloid and lymphoid cell subpopulations. Tumor suspensions were stained with the LIVE/DEAD Fixable Violet Dead Staining Kit (Thermo Fisher Scientific, Inc.) and then labeled with cocktails of fluorochrome-conjugated monoclonal antibodies: anti-CD3 PE-CF594 (clone 145-2C11), anti-CD19 PE-CF594 (clone 1D3) (all from BD Biosciences), anti-NK1.1 PE-Dazzle 594 (clone PK136), anti-CD45 Brilliant Violet 605 (clone 30-F11), anti-CD11b PerCP-Cy5.5 (clone M1/70), anti-CD11c Brilliant Violet 650 (clone N418), anti-F4/80 Alexa Fluor 700 (clone BM8), anti-Ly6C PE (clone HK1.4), anti-Ly6G APC-Cy7 (clone 1A8), anti-MHC II FITC (clone M5/114.15.2) (all from BioLegend) for myeloid cell identification, and anti-CD45 Brilliant Violet 605 (clone 30-F11), anti-CD3 Brilliant Violet 650 (clone 17A2), anti-CD4 FITC (clone RM4-5), anti-CD8 APC/Fire 750 (clone 53-6.7), anti-CD19 Alexa Fluor 700 (clone 6D5), anti-CD25 PE (clone PC61) (all from BioLegend) for lymphocyte identification. Then, cells were fixed using the Foxp3/Transcription Factor Staining Buffer Set (eBioscience). Cells stained with a lymphocyte cocktail were additionally incubated with anti-FoxP3 APC (clone FJK-16s) (eBioscience) monoclonal antibody. The flow cytometry analysis was performed using the

LSR Fortessa flow cytometer with Diva software (BD Biosciences).

Analysis of lymphoid cell populations in spleens obtained from MC38 or B16 F0-tumor bearing mice after applied therapy

Single cell suspensions of spleen cells were thawed and stained for identification of lymphoid cell subpopulations. Spleen suspensions were stained with the LIVE/DEAD Fixable Violet Dead Staining Kit (Thermo Fisher Scientific, Inc.) and then labeled with cocktails of fluorochrome-conjugated monoclonal antibodies: anti-CD45 Brilliant Violet 605 (clone 30-F11), anti-CD3 Brilliant Violet 650 (clone 17A2), anti-CD4 FITC (clone RM4-5), anti-CD8 APC/Fire 750 (clone 53-6.7), anti-CD25 PE (clone PC61), anti-CD62L PerCP-Cy5.5 (clone MEL-14) and anti-CD44 PE-Cy7 (clone IM7) (all from BioLegend). Then, cells were fixed using the Foxp3/Transcription Factor Staining Buffer Set (eBioscience) and sainted with anti-FoxP3 APC (clone FJK-16s) (eBioscience) monoclonal antibody. The flow cytometry analysis was performed using the LSR Fortessa flow cytometer with Diva software (BD Biosciences).

Analysis of the chemotherapeutic' effect on spleen cells representing the systemic anti-tumor immune response

Spleen single cell suspensions (2×10^6 cells) were thawed and cocultured with mitomycin C-treated MC38 or B16 F0 cells (0.1×10^6 cells) in the presence of recombinant human (rh) IL-2 (200 U/ml, ImmunoTools). After 5 days of restimulation, cells were harvested and the cytotoxic activity of effector splenocytes against target (MC38 or B16 F0) cells stained with DiO lipophilic dye (Molecular Probes) was analyzed according to the previously described procedure [29]. The dead target cells were distinguished with propidium iodide (PI, Life Technologies) solution and the percentage of DiO^+PI^+ MC38 or B16 F0 cells was determined. In order to determine the percentage of $CD107a^+$ cells, the degranulation assay was performed. Briefly, restimulated spleen cells were incubated for 2 hours with MC38 or B16 F0 cells in the presence of monoclonal anti-CD107a antibody conjugated with APC (clone 1D4B, BioLegend) together with ionomycin (1 μg/ml, Sigma-Aldrich Merck KGaA), phorbol-12-myristate-13-acetate (50 ng/ml, Sigma-Aldrich Merck KGaA) and rhIL-2 (200 U/ml). Afterwards, cells were harvested and stained with anti-CD45 Brilliant Violet 605 (clone 30-F11), anti-CD4 FITC (clone RM4-5), anti-CD8a APC-Fire750 (clone 53-6.7) and anti-NK1.1 PE-Dazzle 594 (clone PK136) (all from BioLegend). In order to eliminate the dead cells, DAPI dye was used. The flow cytometry analysis was performed using the LSR Fortessa flow cytometer with Diva software (BD Biosciences).

Statistical analyses

All data were analyzed using GraphPad Prism 9 software (GraphPad Software, Inc.). The normality of the residuals was confirmed by the D'Agostino-Pearson omnibus test. When data were consistent with a Gaussian distribution and had equal SD values, the statistical significance was calculated using the parametric one-way ANOVA followed by Tukey's multiple comparison post-hoc test. When data were consistent with a Gaussian distribution, but SD values were not equal the Brown-Forsythe and Welch ANOVA test followed by Dunnett's T3 multiple comparisons post-hoc test was performed. Data inconsistent with a Gaussian distribution were analyzed using the nonparametric Kruskal-Wallis test followed by Dunn's multiple comparison post-hoc test. The statistical significance of tumor growth kinetics was calculated using the two-way ANOVA followed by Tukey's multiple comparisons post-hoc test. The type of statistical analysis used is described in the captions under the figures. All statistically significant differences are presented in the graphs; otherwise, the differences were not significant.

Results

Inhibition of MC38 or B16 F0 tumor growth after therapy with different doses of MTX-based chemotherapeutics

We have previously shown the immunomodulatory potential of HES-MTX nanoconjugate in the murine colon carcinoma MC38 model by observing the beneficial modulation of local and systemic anti-tumor immune response three days after the cytostatic administration [27]. However, we did not evaluate how long over time this effect persists or changes. For this reason, in the current study, we focused both on the dose-dependent therapeutic effec-

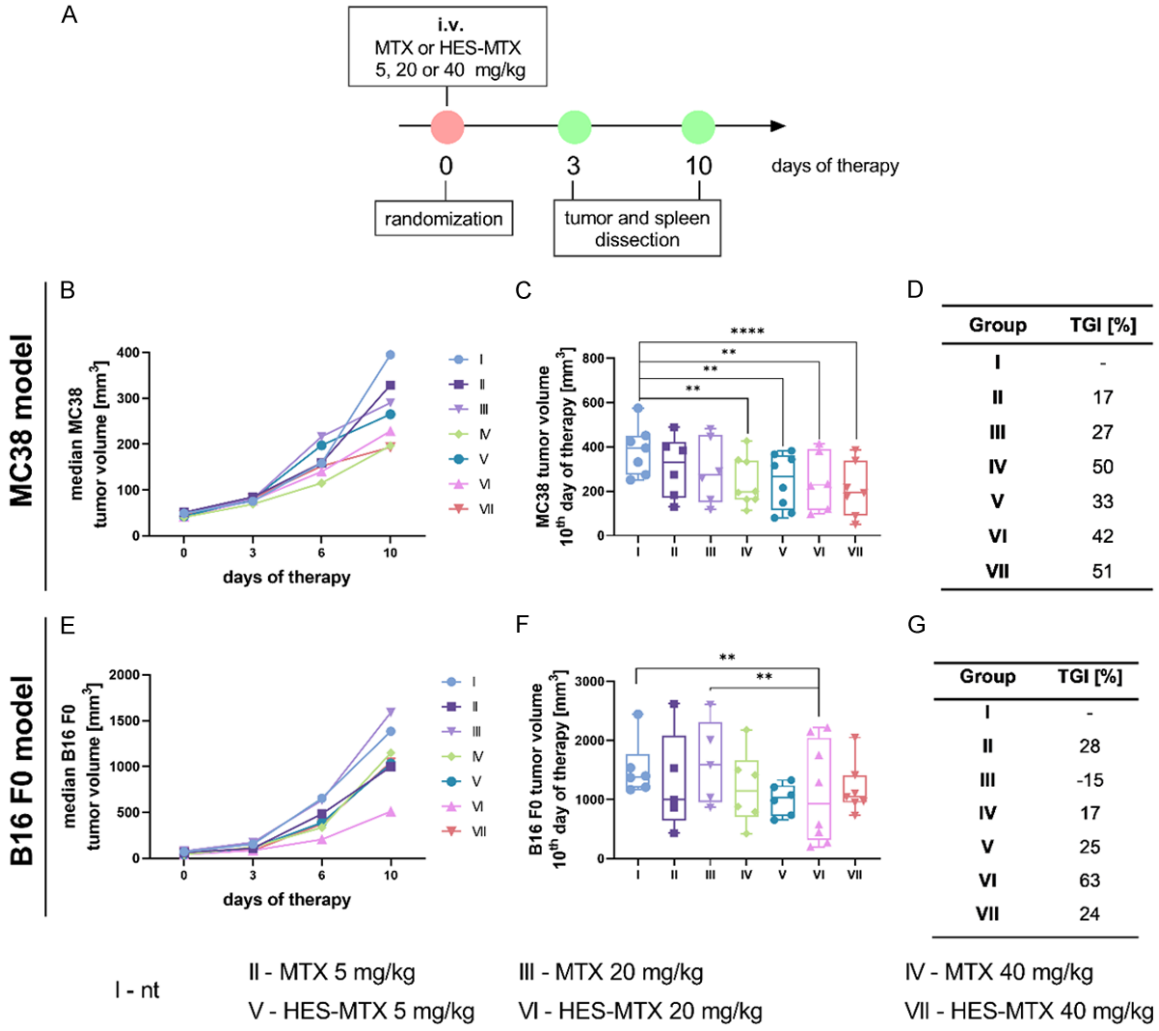

Figure 1. MC38 and B16 F0 tumor growth after chemotherapy with MTX or HES-MTX nanoconjugate. (A) Treatment schedule of therapeutic experiments. (B, E) Graphs presenting MC38 (B) or B16 F0 (E) tumor growth kinetics after chemotherapy. (C, F) Box graph presenting MC38 (C) or B16 F0 (F) tumor volume individual for every mouse in the group with the indicated median for each group on the 10th day of the experiments. Results are presented as a median calculated for 5-7 mice per group. (D, G) Table with the percentage of MC38 (D) or B16 F0 (G) tumor growth inhibition (TGI) calculated on the 10th day of the experiment in relation to the corresponding not treated (nt) group. Differences between groups were estimated using the two-way ANOVA followed by Tukey's multiple comparisons *post-hoc* test (C, F). The asterisks (*) presented in the graphs indicate statistically significant differences between the given groups and the non-treated control group (nt) (**P<0.01; ****P<0.0001).

tiveness of chemotherapy with HES-MTX nanoconjugate in relation to the free form of MTX and the examination of the time-dependent alteration in anti-tumor immune response triggered by used chemotherapeutics. Furthermore, we extended our research with the implementation of another murine tumor model - non-metastatic murine B16 F0 melanoma, which is characterized by faster development and different tumor microenvironment composition, in relation to the MC38 model.

To determine the kinetics of chemotherapy-induced modification of local and systemic immune response in both tumor models, we harvested the tumors and spleens from mice at two-time points - on the 3rd and 10th day of therapy (**Figure 1A**). In the course of the *in vivo* experiments, the tumor volume was measured, and the tumor growth inhibition (TGI) was calculated relative to the corresponding not treated (nt) control group of mice, for the last day of measurement. In the murine colon carcinoma

MC38 model, we observed that the HES-MTX nanoconjugate used at a dose of 5 or 20 mg/kg was more effective in inhibiting tumor growth when compared to the same dose of MTX in free form. In contrast, an administration of the highest dose (40 mg/kg) of both chemotherapeutics resulted in similar tumor growth inhibition revealing the comparable therapeutic efficacy of both agents (**Figure 1B-D**).

For the faster-growing B16 F0 melanoma, at the final measurement point, the median of tumors in the not treated control (nt) group was approx. 10 times higher than in the corresponding group of MC38-bearing mice. Comparing the therapeutic efficacy of administered chemotherapeutics, we found the greatest difference in TGI value for a 20 mg/kg dose. The median of B16 F0 tumor volume in the MTX 20 mg/kg group was greater than in the nt group, whereas the median size of tumor nodules in the HES-MTX 20 mg/kg group was the smallest, and it was reflected also in the calculated TGI value (**Figure 1E-G**). Thus, the dose of 20 mg/kg of HES-MTX in both tumor models caused a greater tumor growth inhibition than MTX in free form (for MC38 tumors the TGI value reached 42%, and for B16 F0 melanoma TGI amounted 63%). Therefore, this dose of the nanoconjugate appeared to be more promising than other tested doses.

Influence of HES-MTX nanoconjugate on the changes in the landscape of tumor-infiltrating lymphoid and myeloid immune cells

Subsequently, we decided to evaluate the immunomodulatory properties of chemotherapeutic agents applied in a 20 mg/kg dose and compare their modifying capacity of the immune response.

With the use of multiparameter flow cytometry analyses, it was possible to evaluate the various immune cell subpopulation in collected tissues. In the population of tumor infiltrating $CD45^+$ leukocytes, we identified the myeloid and lymphoid immune cells (**Figure 2A**). Among the $CD45^+$ cells infiltrating tumors, the percentage of MDSCs ($CD11b^+CD11c^-F4/80^-Ly6C^+$) was determined, and additionally, based on expression of Ly6G molecule of their surface, it was possible to distinguish two distinct MDSC subpopulations: monocytic (M-) MDSCs ($Ly6C^+Ly6G^-$) and polymorphonuclear (PMN-)MDSCs ($Ly6C^{int}Ly6G^+$). The size of the TAM population ($CD11b^+CD11c^+F4/80^+$) was also investigated and based on the surface MHC II expression - the activation level of these cells. The percentage of DCs ($CD11b^+CD11c^+F4/80^{int}MHC\ II^+$) and their activation level (expression of MHC II and CD80 surface molecules) were determined in tumors. The subpopulations of lymphoid immune cells were also distinguished: CD4 T cells ($CD3^+CD4^+$), regulatory T lymphocytes ($CD3^+CD4^+CD25^+FoxP3^+$), CD8 T cells ($CD3^+CD8^+$), NK ($CD45^+CD3^-NK1.1^+$) and NKT cells ($CD3^+NK1.1^+$).

On the 3rd day after the application of HES-MTX, a significantly increased influx of $CD45^+$ leukocytes into MC38 tumors was noted. On the 10th day, the percentage of these cells remained at a similar level, but the differences were no longer statistically significant (**Figure 2B**). Admittedly a similar level of $CD45^+$ cell influx induced by the nanoconjugate was observed at both time points, but the use of summary graphs representing the normalized data of all analyzed immune cell subpopulations in MC38 tumors allowed us to note the chemotherapeutic-related changes in the TME immune cell landscape during the progression of the tumor (**Figure 2C**, **2D**).

On the 3rd day of therapy, the percentage of leukocytes in the untreated control groups was similar in both tumor models. However, in the melanoma model, the chemotherapeutic application did not enhance the influx of $CD45^+$ cells into the tumor tissue. In turn, one week later, unlike in colon cancer, the size of the immune cell influx into B16 F0 tumors was significantly diminished. This was presumably associated with the rapid growth of B16 F0 tumor nodules. Even more, the use of HES-MTX caused a significant decrease in the percentage of leukocytes in tumors when compared to the MTX-treated group of mice (**Figure 2E**). Although the influx of $CD45^+$ cells into the tissue of B16 F0 tumors was significantly reduced, summary graphs with the normalized percentage of all analyzed immune cell subpopulations revealed chemotherapeutic-dependent changes in the size in MDSC and $CD4^+$ cell populations (**Figure 2F**, **2G**).

Comparing MDSC populations infiltrating the MC38 tumor tissue, we revealed that neither the type of chemotherapeutic used nor the

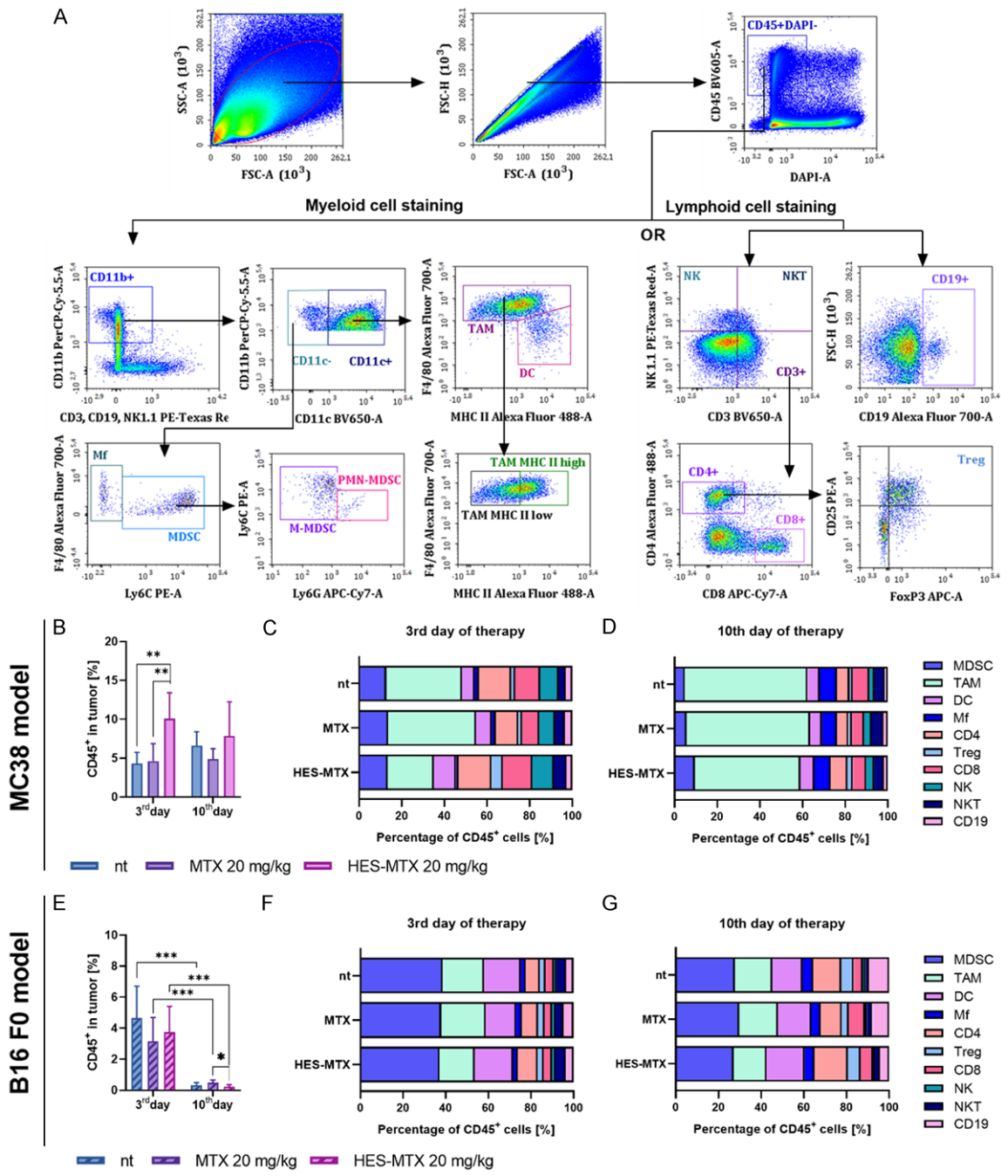

Figure 2. Impact of chemotherapy on the infiltration of MC38 or B16 F0 tumor nodules with leukocytes and overall landscape of immune cells in TME. (A) Scheme of the multiparameter flow cytometric analysis of lymphoid and myeloid cells in tumor tissue. (B, E) Percentage of live CD45$^+$ cells in tumor tissue. (C, D, F, G) Percentage of each leukocyte population on the (C, F) 3rd or (D, G) 10th day of the experiment. Results are presented as mean + SD calculated for 3-7 mice per group. Differences between groups were estimated using the parametric one-way ANOVA followed by Tukey's multiple comparisons *post-hoc* test (B, E). The asterisks (*) presented in the graphs over the lines indicate a statistically significant differences between the given groups (*P<0.05; **P<0.01; ***P<0.001).

level of MC38 tumor development significantly affected the size of the M-MDSC subpopulation (**Figure 3A**). But the percentage of PMN-MDSCs increased after therapy with MTX, on the 3rd day of therapy, and after the use of HES-MTX increased on the 10th day of therapy (**Figure 3B**). TAMs constituted the most abundant subpopulation of all leukocytes present in

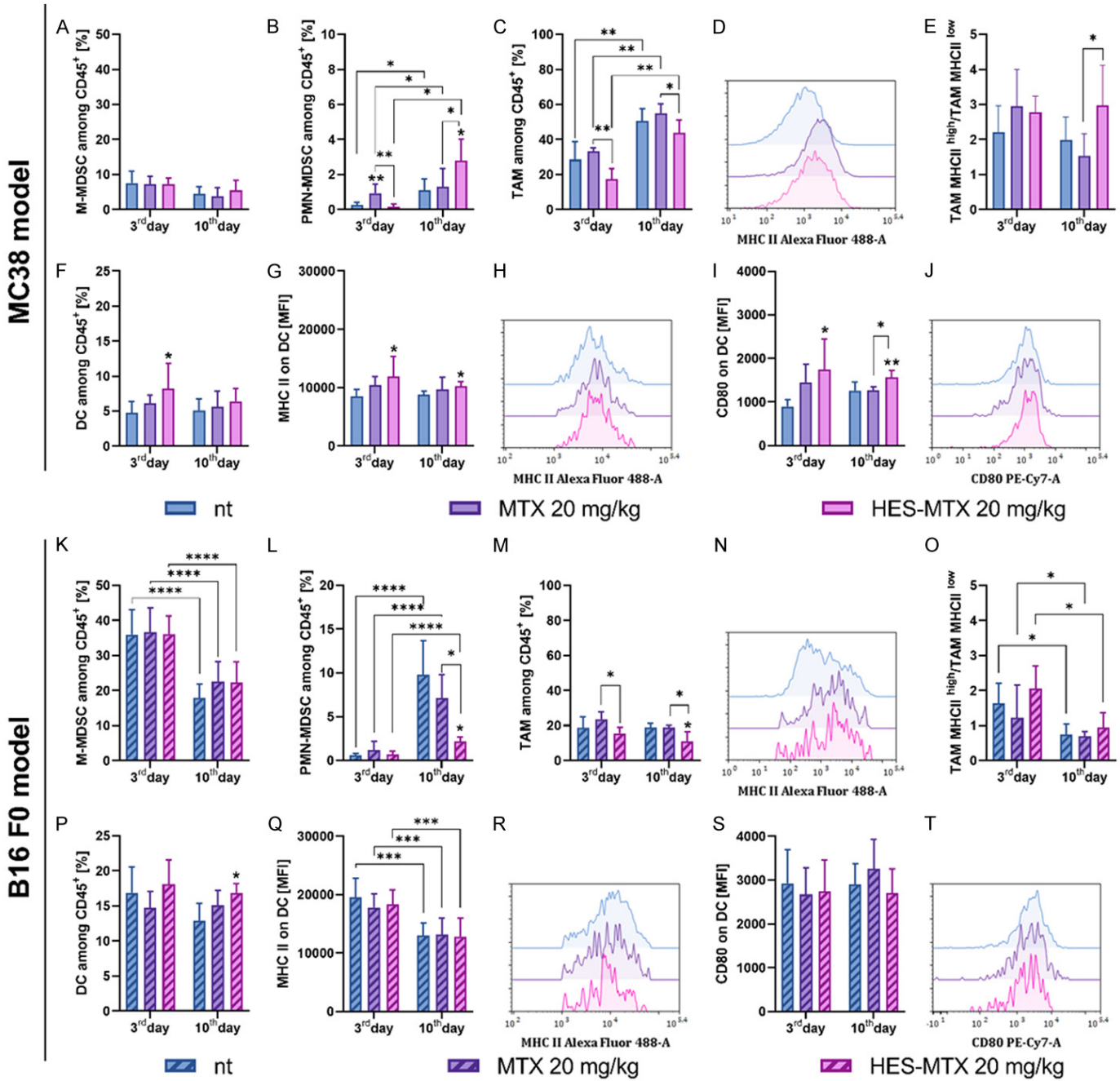
MC38 model
B16 F0 model
A
B
C
D
E
F
G
H
I
J
K
L
M
N
O
P
Q
R
S
T
M-MDSC among CD45+ [%]
PMN-MDSC among CD45+ [%]
TAM among CD45+ [%]
TAM MHCII high/TAM MHCII low
DC among CD45+ [%]
MHC II on DC [MFI]
CD80 on DC [MFI]
3rd day
10th day
MHC II Alexa Fluor 488-A
CD80 PE-Cy7-A
nt
MTX 20 mg/kg
HES-MTX 20 mg/kg

Figure 3. Influence of applied chemotherapy on the tumor-infiltration of myeloid immune cells in MC38 or B16 F0 tumors. Percentage of M-MDSC (A, K), PMN-MDSC (B, L) or TAM (C, M) among $CD45^+$ cells in tumors. Representative histogram showing the expression of MHC II (D, N) on TAM surface. TAM MHC II^{high}/TAM MHC II^{low} (E, O) ratios showing the polarization of TAMs in tumor tissue. Percentage of DC (F, P) among $CD45^+$ cells in tumors. Expression of MHC II (G, Q) or CD80 (I, S) on DC surface. Representative histogram showing the expression of MHC II (H, R) or CD80 (J, T) on the DC surface. Results are presented as mean + SD calculated for 3-7 mice per group. Differences between groups were estimated using the non-parametric Kruskal-Wallis test followed by Dunn's multiple comparisons *post-hoc* test (C, F, G, I), the parametric one-way ANOVA followed by Tukey's multiple comparisons *post-hoc* test (B, C, E, I, K-M, O-Q) or the parametric Brown-Forsythe and Welch ANOVA test followed by Dunnett's T3 multiple comparisons *post-hoc* test (L). The asterisks (*) presented above the bars indicate statistically significant differences between the given groups and the non-treated control group (nt). The asterisks (*) over the lines indicate statistically significant differences between the given groups (*P<0.05; **P<0.01; ***P<0.001; ****P<0.0001).

the MC38 tumor nodules and the size of their subpopulation increased significantly during tumor development. Nevertheless, in relation to the MTX-treated group of mice, the application of HES-MTX nanoconjugate caused a long-lasting reduction in the percentage of TAMs (**Figure 3C**). We also analyzed the activation level of these cells based on the surface expression of the MHC II molecule (**Figure 3D**), finding a significant increase TAM MHC II^{high}/TAM MHC II^{low} ratio after the nanoconjugate use, but only on the 10^{th} day of therapy (**Figure 3E**). Another subpopulation of myeloid cells was DCs, whose activation level has been also specified. Three days after HES-MTX administration, the increased influx of DCs into MC38 tumors was noted. Although this state did not persist over time, the use of nanoconjugate caused a sustained enhancement in the activation degree of DCs, which was exhibited in the increased expression of MHC II and CD80 molecules on the surface of those cells (**Figure 3F-J**).

In the case of B16 F0 tumors, flow cytometry analyses of myeloid cell subpopulations showed a different landscape of TME. Unlike the colon cancer model, MDSCs were the most abundant population of immune cells among $CD45^+$ leukocytes infiltrating B16 F0 tumors. Within this population, time-dependent changes in the proportion of M-MDSC and PMN-MDSC were found. Three days after chemotherapeutic administration, no changes were observed in the percentage of M-MDSC in comparison to the control group, but one week later this subpopulation decreased to half in all groups (**Figure 3K**). An inverse relationship was observed in the PMN-MDSCs' subpopulation - tumor development was accompanied by a significant increase in the percentage of these cells. On the 3^{rd} day of therapy, the impact of applied chemotherapeutics on the size of the PMN-MDSCs subpopulation was not found. However, one week later, in the HES-MTX-treated group of mice, a reduction in the percentage of this cell subpopulation was demonstrated and this change was statistically significant when compared to the control and MTX groups of mice (**Figure 3L**). Unlike the MC38 tumor model, the size of TAMs' subpopulation in B16 F0 tumors remained at similar levels at both time points. After administration of HES-MTX nanoconjugate, we observed a sustained reduction in the percentage of TAMs, however, this change was not accompanied by significant alterations in the value of TAM MHC II^{high}/TAM MHC II^{low} ratio (**Figure 3M-O**). On the 3^{rd} day of therapy, the influx of DCs into B16 F0 tumor tissue was at the same level regardless of the applied chemotherapeutics. However, on the 10^{th} day, we observed an increase in the DC percentage caused by the HES-MTX nanoconjugate (**Figure 3P**). The evaluation of the activation level of those cells did not show any chemotherapeutic-dependent changes in the expression of MHC II and CD80 molecules on the surface of DCs infiltrating the B16 F0 tumor tissue (**Figure 3Q-T**).

The changes in the size of lymphoid cell subpopulations caused by used chemotherapy were visible in both tumor models. In the course of MC38 tumor progression, the percentage of $CD4^+$ cells decreased and none of the applied chemotherapeutics affected this process (**Figure 4A**). Three days after starting therapy approximately 40% of all $CD4^+$ cells found in these tumors were identified as regulatory T cells, but one week later, their percentage significantly decreased regardless of the chemotherapeutic use (**Figure 4B**). However, in the case of $CD8^+$ cells, the short-term impact of the HES-MTX nanoconjugate was revealed - on the

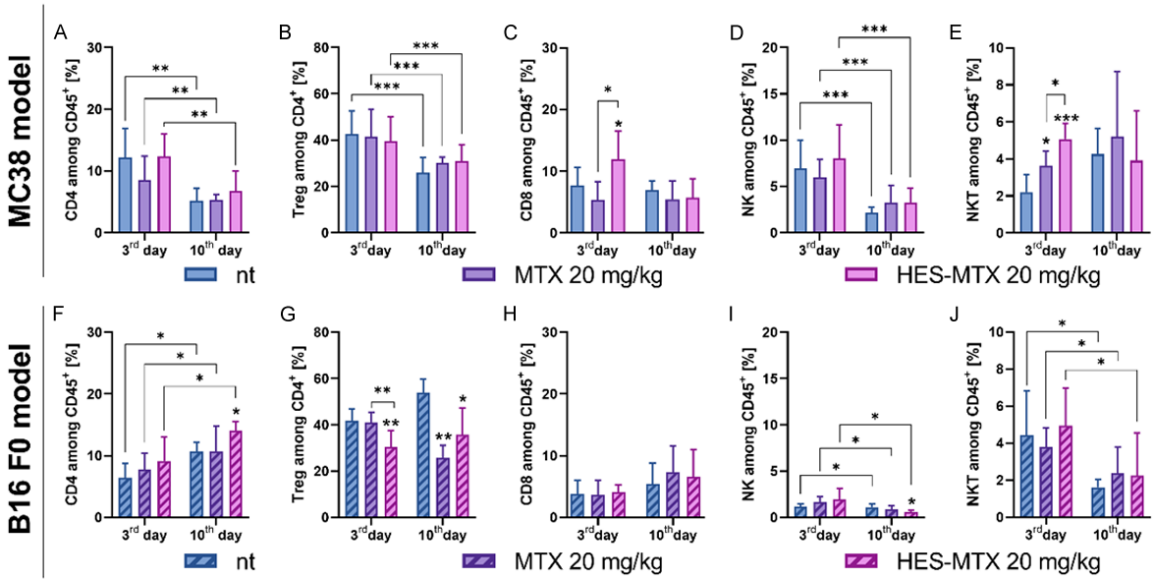

Figure 4. Influence of applied chemotherapy on the tumor-infiltration and activation status of lymphoid immune cells in MC38 or B16 F0 tumors. Percentage of $CD4^+$ (A, F), $CD8^+$ (C, H), NK (D, I) and NKT cells (E, J) among $CD45^+$ cells in the tumor. Percentage of T regulatory lymphocytes among $CD4^+$ cells in tumor tissue (B, G). Results are presented as mean + SD calculated for 3-7 mice per group. Differences between groups were estimated using the parametric one-way ANOVA followed by Tukey's multiple comparisons *post-hoc* test (A-E, I, J) or the parametric Brown-Forsythe and Welch ANOVA test followed by Dunnett's T3 multiple comparisons *post-hoc* test (F). The asterisks (*) presented above the bars indicate statistically significant differences between the given groups and the non-treated control group (nt). The asterisks (*) over the lines indicate statistically significant differences between the given groups (*P<0.05; **P<0.01; ***P<0.001).

3rd day of therapy the percentage of $CD8^+$ cells significantly elevated compared with other groups of mice, but this effect was not maintained (**Figure 4C**). In the case of NK cells, similar changes during the tumor progression were observed. The effect of the applied therapy on the NK population size was not observed, while the degree of NKT cells infiltration into MC38 tumors was affected by both chemotherapeutics, especially the HES-MTX treatment. Despite the fact, that this effect was limited only to the 3rd day of the therapy, it should be mentioned that HES-MTX caused the highest influx of NKT cells into tumors when compared to the not treated and MTX-treated groups of mice (**Figure 4D**, **4E**).

Opposite to the previous tumor model, the rapid development of B16 F0 tumor nodules was accompanied by an increase in the $CD4^+$ cells percentage. The chemotherapeutic-dependent effect on the size of the $CD4^+$ population was observed only on the 10th day of therapy when the influx of $CD4^+$ cells was the greatest in the HES-MTX-treated group (**Figure 4F**). Moreover, therapy with HES-MTX caused a long-lasting decrease in the percentage of Tregs among $CD4^+$ cells compared to the nt control group. The MTX-induced reduction in the Tregs subpopulation size was also noted, however, in this case, the decrease in the percentage was observed at a later time point (**Figure 4G**). Analyzing $CD8^+$ cell infiltration into B16 F0 tumor tissue, we did not observe any alterations in the percentage of these cells, neither dependent on the development of the tumor nor on the applied chemotherapeutics (**Figure 4H**). Among all identified lymphoid immune cells, the fast growth of the B16 F0 tumor also caused a strong reduction in the NK and NKT percentages. However, only 10 days after administration of HES-MTX a significant decrease in the size of the NK cell subpopulation relative to the control group was observed (**Figure 4I**, **4J**).

The obtained data indicate that in contrast to the use of MTX in a free, unconjugated form, the therapy with HES-MTX resulted in the modulation of local immune response in both analyzed murine tumor models. However, due to the different rates of tumor development and

the diversity of the TME in both tumors, the observed immunomodulation involved different populations of immune cells and additionally had different kinetics of occurrence.

In the MC38 tumor model, the most beneficial changes in the landscape of TME were noted on the 3rd day of therapy - shortly after the administration of HES-MTX. On the one hand, the long-lasting reduction in the percentage of TAMs was accompanied by the final domination of these cells with high MHC II expression, and on the other, an increased influx of highly activated DCs into MC38 tumors, was observed. It should be mentioned that the percentage of PMN-MDSCs significantly increased after the therapy with HES-MTX on the 10th day of therapy. The immunomodulation among the lymphoid cells was visible in the temporarily increased infiltration of $CD8^+$ and NKT cells to tumor nodules.

In turn, in the case of the B16 F0 model, the majority of observed changes occurred on the 10th day of therapy with HES-MTX nanoconjugate. As a result of this therapy, these tumors were less infiltrated by cells with suppressor activity such as PMN-MDSCs, TAMs and Tregs. However, for the latter two subpopulations, the effect was already noticeable shortly after nanoconjugate administration. Moreover, this type of therapy resulted in a greater influx of DCs into tumor nodules, but the phenotype characteristic of these cells did not indicate that the applied therapy increased their degree of activation. The changes among the activated lymphoid cell subpopulations demonstrate that in B16 F0 tumors, the main immunomodulatory influence of HES-MTX nanoconjugate was focused on the postponed increased infiltration of $CD4^+$ cells, rather than other lymphoid immune cells.

The impact of therapy with HES-MTX nanoconjugate on the activation of specific systemic anti-tumor immune response

The effect on the local immune response induced by applied chemotherapeutics, especially HES-MTX, was reflected in the changes in the size and activity of immune cells at the systemic immune response level. With the use of multiparameter flow cytometry analyses, it was possible to identify and determine the size of various lymphoid cell subpopulations in spleens collected from tumor-bearing mice (**Figure 5A**). We observed the tumor-type-dependent diversity of immune response kinetics in the landscape of splenic lymphoid cells, especially in the groups of mice treated with HES-MTX compared to not treated mice.

In the MC38 tumor model, most of the changes in the size of the individual lymphoid cell population were evident on the 3rd day after the administration of chemotherapeutics. The use of MTX caused a significant reduction in the percentage of $CD4^+$ cells compared to the control group at this time point. However, therapy with HES-MTX, resulted in an enlargement in the size of the $CD4^+$ cell subpopulation, as well as an increase in the percentages of effector and memory $CD4^+$ cells (**Figure 5B-D**). On the other hand, the use of HES-MTX contributed to the temporary increase in the percentage of Tregs, which was accompanied by elevation in the percentage of memory Tregs, while the size of effector Treg remained unchanged (**Figure 5E-G**). The modulation of immune response by nanoconjugate can be also found in the enlargement in the $CD8^+$ cells percentage. Three days after administration of HES-MTX, the size of the $CD8^+$ cell population was significantly elevated compared to the control and MTX-treated groups of mice. On the 10th day of therapy, in the HES-MTX group of mice, the percentage of $CD8^+$ cells was the highest. The activation status of splenic effector $CD8^+$ cells was not affected by applied chemotherapeutics, however, the size of the memory cell population significantly decreased in response to HES-MTX (**Figure 5H-J**). The used chemotherapeutics did not change the size of the NK cell subpopulation compared to the control group, nevertheless, the percentage of splenic NKT cells gradually increased in the HES-MTX-treated group of mice (**Figure 5K**, **5L**).

Unlike the MC38 tumor model, in the case of spleens obtained from B16 F0-bearing mice, the chemotherapeutic-related changes in the size of immune cell subpopulations were observed on the 10th day of therapy. In a group of mice treated with MTX, a decrease in the percentage of $CD4^+$ cells in relation to the control group was found in both time points. The nanoconjugate application caused a significant increase in the $CD4^+$ cell percentage but only on the 10th day of therapy (**Figure 5M**).

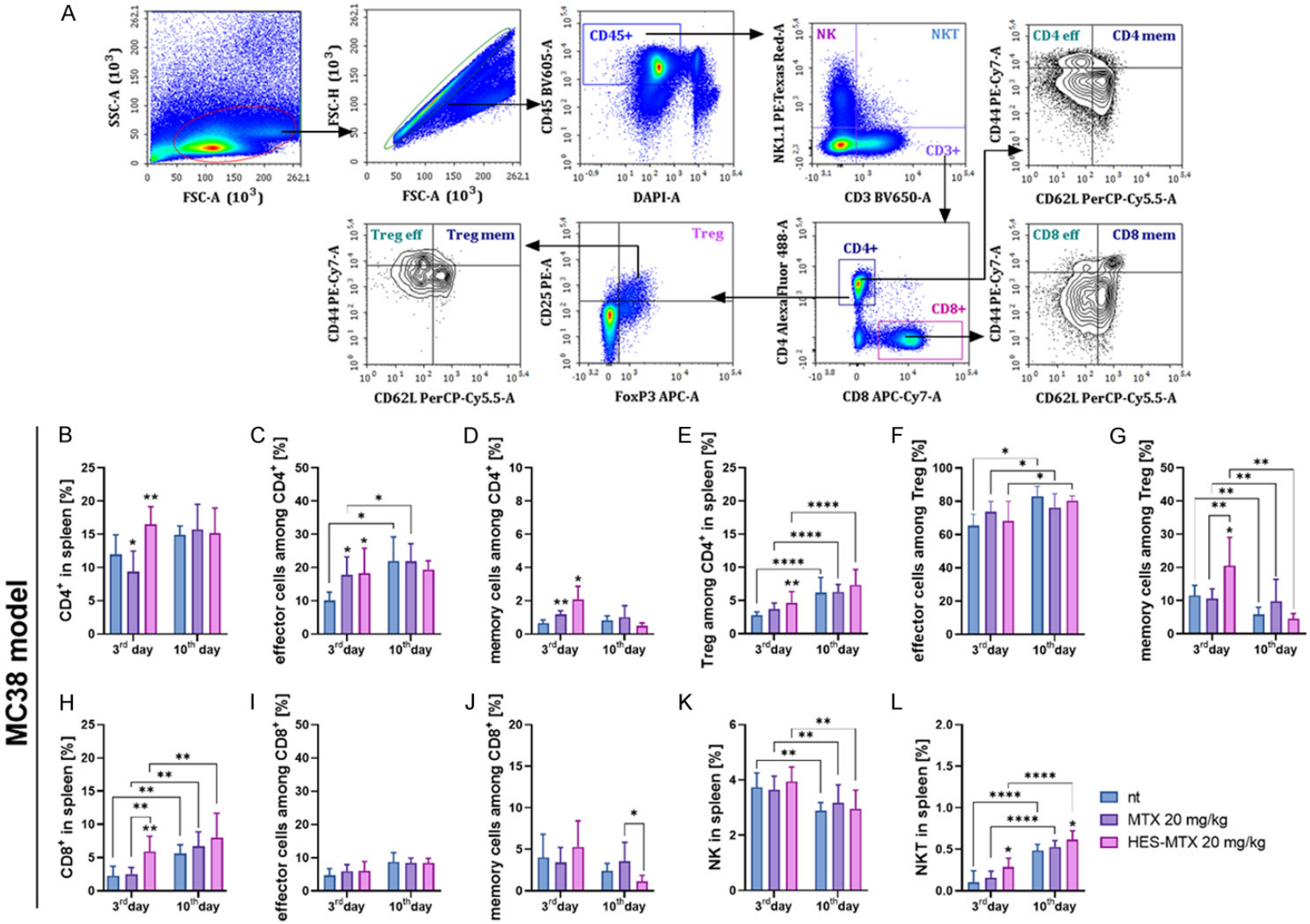
A
SSC-A (10^3)
FSC-A (10^3)
FSC-H (10^3)
CD45+
CD45 BV605-A
DAPI-A
NK
NKT
CD3+
NK1.1 PE-Texas Red-A
CD3 BV650-A
CD4 eff
CD4 mem
CD44 PE-Cy7-A
CD62L PerCP-Cy5.5-A
Treg eff
Treg mem
Treg
CD25 PE-A
FoxP3 APC-A
CD4+
CD8+
CD4 AlexaFluor 488-A
CD8 APC-Cy7-A
CD8 eff
CD8 mem
MC38 model
B
CD4+ in spleen [%]
C
effector cells among CD4+ [%]
D
memory cells among CD4+ [%]
E
Treg among CD4+ in spleen [%]
F
effector cells among Treg [%]
G
memory cells among Treg [%]
H
CD8+ in spleen [%]
I
effector cells among CD8+ [%]
J
memory cells among CD8+ [%]
K
NK in spleen [%]
L
NKT in spleen [%]
3rd day
10th day
nt
MTX 20 mg/kg
HES-MTX 20 mg/kg

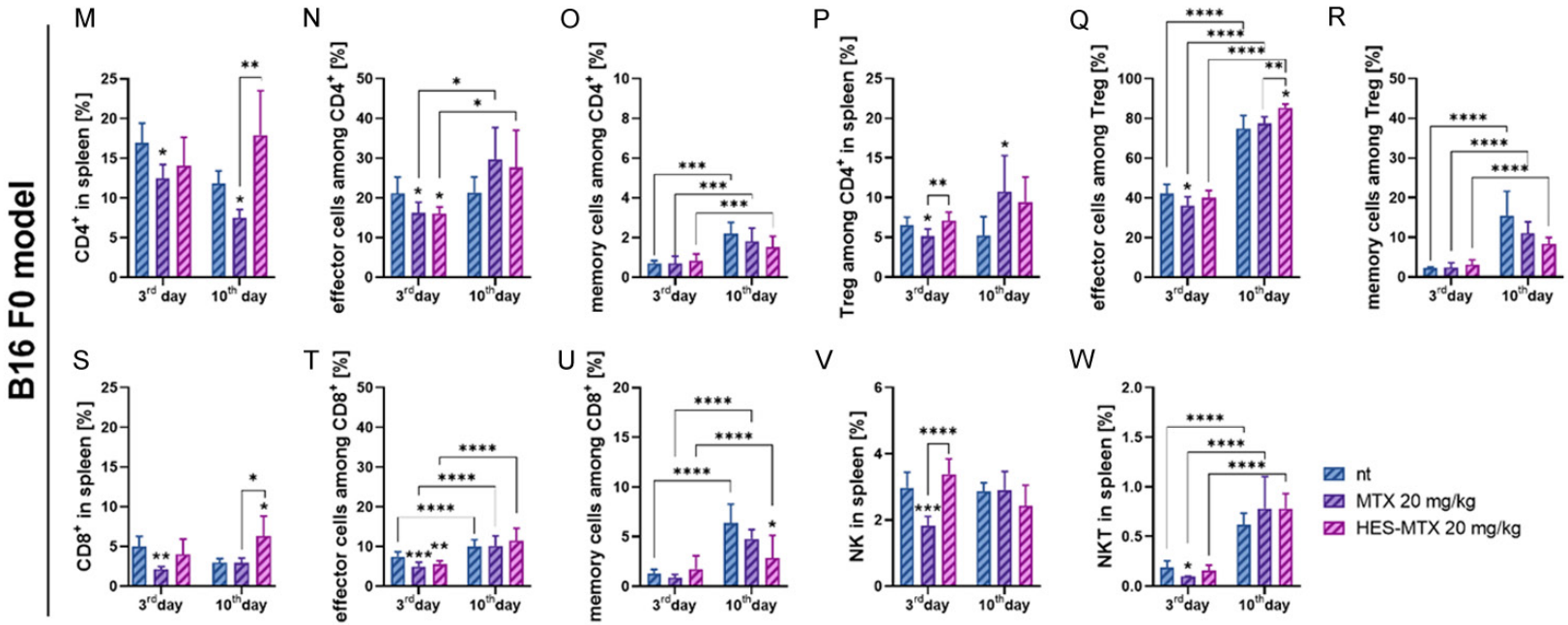

Figure 5. Effect of applied therapy on size and the activation level of the lymphocytes in the spleen obtained from MC38- or B16 F0-bearing mice treated with MTX or HES-MTX nanoconjugate. (A) Scheme of the multiparameter flow cytometric analysis of lymphoid cells among splenocytes. (B, M) Percentage of $CD4^+$ cells among splenocytes. Percentage of effector cells (C, N), memory cells (D, O), and Treg cells (E, P) among $CD4^+$ cells in the spleen. Percentage of effector cells (F, Q) and memory cells (G, R) among Treg. (H, S) Percentage of $CD8^+$ cells in the spleen. Percentage of effector (I, T) and memory cells (J, U) among $CD8^+$. Percentage of NK (K, V) and NKT cells (L, W) in spleen. Results are presented as mean + SD calculated for 3-7 mice per group. Differences between groups were estimated using the parametric one-way ANOVA followed by Tukey's multiple comparisons *post-hoc* test (B, C, E-H, K-W), the parametric Brown-Forsythe and Welch ANOVA test followed by Dunnett's T3 multiple comparisons *post-hoc* test (D, Q, S) or the non-parametric Kruskal-Wallis test followed by Dunn's multiple comparisons *post-hoc* test (C, E, J, M). The asterisks (*) presented above the bars indicate statistically significant differences between the given groups and the non-treated control group (nt). The asterisks (*) over the line indicate statistically significant differences between the given groups (*P<0.05; **P<0.01; ***P<0.001; ****P<0.0001).

Substantial changes in the activation level of these cells were noted after the use of both types of chemotherapeutics. On the 3rd day of therapy, a decrease in effector $CD4^+$ cell percentage was observed, but at the final time point, the size of both populations effector and memory $CD4^+$ cells was characterized by a significant increase compared to the previous time point (**Figure 5N**, **5O**). Shortly after the MTX administration into B16 F0-tumor bearing mice a decrease in Treg percentage was observed, but on the 10th day of therapy, the size of this cell population was the highest. In the group of mice receiving HES-MTX, initially, the percentage of splenic Tregs was at the same level as the control group, however, one week later, the size of Tregs percentage was insignificantly increased. Taking into consideration the activation status of these cells, the only chemotherapeutic-related differences were found in the population of effector cells. Although initially the use of MTX caused a decrease in the population size of effector Tregs, on the 10th day of therapy, the percentage of these cells reached a level similar to the control group. Administration of HES-MTX resulted, at this time point, in a strong elevation of the percentage of effector Tregs (**Figure 5P-R**). Similar to the previously discussed splenic $CD4^+$ immune cells, administration of MTX caused initially, a temporary reduction in the percentages of $CD8^+$, but also NK and NKT cells, when compared to the nt group of mice (**Figure 5S**, **5V**, **5W**). However, the only effect of the nanoconjugate on the alterations in the size of these cell subpopulations was visible in the case of $CD8^+$ cells, the percentage of which significantly increased on the 10th day of therapy. Among splenic $CD8^+$ cells, the decrease in the percentage of effector cells was noted on the 3rd day of therapy in both treated groups of mice, whereas, in the case of memory cells, a significant reduction in the size of these cells was found on 10th day after HES-MTX application (**Figure 5T**, **5U**).

To determine the impact of both chemotherapeutics on the activation of the anti-tumor immune response, the *ex vivo* restimulation of spleen cells was performed. In such functional assay, splenocytes that have had first contact with antigens in tumor-bearing mice were secondary *ex vivo* stimulated with tumor antigens derived from tumor cell lines. The restimulation made it possible to detect the direction of development of a specific immune response, as well as to assess the ability of different populations of splenic lymphoid cells to secrete cytolytic $CD107a^+$ granules. These results were additionally supplemented by the determination of the indirect cytotoxic activity of spleen cells against tumor cells.

In the MC38 tumor model, restimulation of splenocytes collected 3 days after administration of HES-MTX resulted in a significant increase in the percentage of $CD8^+$ cells compared to MTX-treated mice, while subpopulations of $CD4^+$ and NK cells remained unchanged. It is worth mentioning that, despite the lack of alterations in the size of the latter cell subpopulation, the degranulation assay revealed a significantly higher percentage of NK $CD107a^+$ cells. At this time point, in the HES-MTX-treated group, the ability of $CD4^+$ and $CD8^+$ cells to secrete cytolytic granules was the lowest and the highest respectively, but these alterations were not statistically significant. However, restimulation of splenocytes harvested on the 10th day of therapy showed the switch in the type of anti-tumor immune response - in a nanoconjugate-treated group of mice we observed on the one hand, the reduction in the percentages of $CD4^+$ and $CD8^+$ cells, and increase in the size of NK cell subpopulation, on the other. Taking into consideration their ability to degranulation, the increased percentage of $CD107a^+$ cells was found only for $CD4^+$ cells. In other cases - the $CD8^+$ and NK cells had a reduced capacity to release cytolytic granules (**Figure 6A-F**). The confirmation of these observations can be also found in the cytotoxic activity of restimulated splenocytes. On the 3rd day of therapy, the greatest ability of spleen cells to eliminate MC38 cells was observed in the HES-MTX group of mice. This was indirectly associated with an increased percentage of $CD8^+$ cells after restimulation, as well as with enhanced capacity of $CD8^+$ and NK cells to degranulate, which was observed at that time point. However, increased cytotoxic activity was only temporary, because on the 10th day of therapy, no treatment-related changes were found (**Figure 6G**).

In the B16 F0 tumor model, as a result of the secondary contact of spleen cells with the tumor cells, the domination of NK-dependent

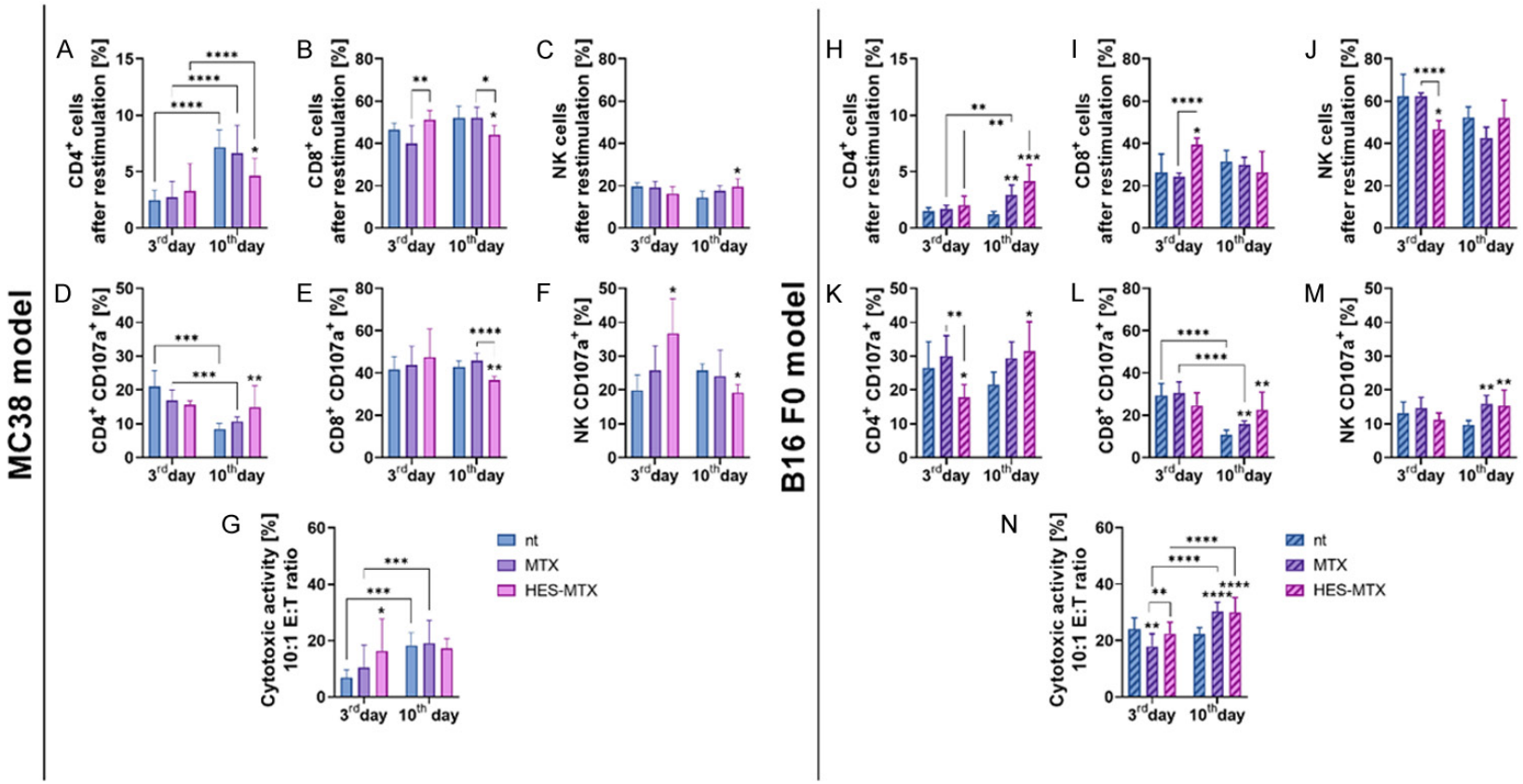

Figure 6. Impact of chemotherapy with MTX or HES-MTX nanoconjugate on the induction of systemic anti-tumor response in MC38 or B16 F0-tumor bearing mice. Percentage of (A, H) $CD4^+$, (B, I) $CD8^+$, and (C, J) NK cells among restimulated splenocytes. Percentage of $CD107a^+$ cells among (D, K) $CD4^+$, (E, L) $CD8^+$ and (F, M) NK cells. Cytotoxic activity of splenocytes (effector cells, E) against DiO^+ MC38 cells (target cells, T) after 4-hour incubation in 10:1 (G, N) E:T ratio measured using flow cytometry. Results are presented as mean + SD calculated for 3-7 mice per group. Differences between groups were estimated using the parametric one-way ANOVA followed by Tukey's multiple comparisons *post-hoc* test (A-E, G-I, L, M), the parametric Brown-Forsythe and Welch ANOVA test followed by Dunnett's T3 multiple comparisons *post-hoc* test (H-K, M, N) or the non-parametric Kruskal-Wallis test followed by Dunn's multiple comparisons *post-hoc* test (B, D, F-H). The asterisks (*) presented above bars indicate statistically significant differences between the given groups and the non-treated control group (nt). The asterisks (*) over the lines indicate statistically significant differences between the given groups (*P<0.05; **P<0.01; ***P<0.001; ****P<0.0001).

type of immune response was noted, instead of $CD8^+$ cells, which was observed in MC38 tumors. On the 3rd day of therapy, despite there were no changes in the percentage of $CD4^+$ cells, the use of HES-MTX caused a significant enlargement in the size of $CD8^+$ cells on the one hand, and the reduction in the percentage of NK cells on the other. However, after restimulation of splenocytes collected on the 10th day of therapy, the main effect of administered chemotherapeutics on alterations in the percentage of individual immune cells was visible only in the case of $CD4^+$ cells. The increase in the size of their subpopulation was observed in both treated groups of mice, but the highest percentage was revealed in the group which received HES-MTX. At this time point, no chemotherapeutic-dependent changes in the size of the $CD8^+$ and NK cell subpopulations were noticed (**Figure 6H-J**). The evaluation of the capacity of cytolytic granules' secretion demonstrated that the most advantageous changes in the percentage of $CD107a^+$ cell population involved spleens collected on the 10th day of therapy. At that time, we observed an increase in the size of $CD107a^+$ cells among $CD4^+$, $CD8^+$ and NK cells in both treated group of mice, nevertheless, the highest percentages of $CD4^+CD107a^+$ and $CD8^+CD107a^+$ cells was noted in the group of mice receiving HES-MTX (**Figure 6K-M**). Moreover, the variations in the degranulation ability of restimulated splenocytes were also reflected in the increased capacity of these cells to eliminate the tumor B16 F0 cells as a result of their direct cell-to-cell contact. In comparison to the control nt group of mice the increased cytotoxic activity was observed for spleen cells collected 10 days after starting the therapy, although it is worth adding that there were no differences in the cytotoxic activity between both chemotherapeutics (**Figure 6N**).

Based on the assessment of the systemic anti-tumor immune response, we conclude that the changes among the tumor lymphoid immune cell subpopulations were also reflected in the changes among the splenic lymphoid immune cells, regardless of the tumor model. More precisely, in the MC38 model it was confirmed that the induced by HES-MTX immunomodulation mainly occurred on the 3rd day of therapy and concerned the increased percentage of splenic $CD8^+$ and NKT cells, but for the latter subpopulation of cells, this effect was long-lasting. Moreover, in contrast to the local immune response, the immunomodulatory effect of HES-MTX was also applied to the splenic $CD4^+$ cells, whose percentage was increased. In the B16 F0 tumor model, the significant changes in the landscape of splenic lymphoid cells were revealed on the 10th day after HES-MTX administration and were mainly concerned with the increase in the $CD4^+$ and $CD8^+$ cells. Similar to the previous model, the influence of nanoconjugate on the size of the $CD8^+$ cell population was visible only at the systemic immune response level.

Moreover, considering the ability of splenocytes to activate the antigen-specific immune response it can be concluded that the nanoconjugate-induced alterations both at the local and systemic immune response, were also reflected in the changes in the degranulation capacity of restimulated spleen cells, which was additionally confirmed by the higher cytotoxic activity of these cells against tumor cells.

Discussion

In the present work, we demonstrated the immunomodulatory potential of MTX-based nanoconjugate in two different murine tumor models - MC38 colon carcinoma and B16 F0 melanoma. This study is a continuation and extension of our previous research [27] with the use of nanoconjugate of methotrexate (MTX) as an anticancer agent and hydroxyethyl starch (HES), as a high-molecular carrier, applied in the therapy of MC38- and B16 F0-tumor bearing mice. The use of HES-MTX nanoconjugate in a dose of 20 mg/kg caused the significant inhibition of tumor growth in both tumor models and also revealed the time-dependent beneficial influence on the local and systemic anti-tumor immune response. Furthermore, by evaluating changes in immune response occurring over time and by detailed characteristics of various immune cell subpopulations involved in the creation of this response, it was possible to define when and which immune cells were the most activated by the use of HES-MTX nanoconjugate and to determine how it was related to an observed delay of tumor growth.

In both tested cancer models, it was noticed that the HES-MTX therapy at a dose of 20 mg/

kg caused a much greater slowdown of cancer development than MTX in free form. The median MC38 tumor volume in the group of mice receiving HES-MTX was 42% smaller, whereas in the case of B16 F0 tumors - the tumor nodules were 63% smaller than in the corresponding control group. For comparison - after therapy with 20 mg/kg of MTX the calculated TGI values were 27% for MC38 and -15% for the B16 F0 tumor model. This phenomenon of increased therapeutic efficacy of HES-MTX over its unconjugated counterpart was also previously reported in the MC38 tumor model [27, 31] as well as in murine P388 and human MV-4-11 leukemia models [23]. Moreover, in the case of other types of MTX-based conjugates, similar observations have been reported. For instance, the conjugate of MTX with hydroxyethylcellulose [32] or with glucose [33] was more efficient in the inhibition of 4T1 murine breast tumor development when compared to the therapy with MTX in free form. However, in the current research, besides confirming the greater anti-tumor activity of the HES-MTX nanoconjugate in the MC38 and B16 F0 tumor models, we additionally provide a comprehensive explanation of the changes in the anti-tumor immune response caused by the administration of HES-MTX, which finally led to the demonstrated beneficial therapeutic effect.

Based on obtained results from the local anti-tumor immune response, it can be concluded that the immunomodulatory potential of HES-MTX nanoconjugate may be closely related to the specific immune cell composition of the tumor microenvironment. This determines not only when the immunomodulation phenomenon occurs, but also indicates which cell populations will undergo these changes. In this regard, one of the main differences between the two analyzed tumor models concerned the kinetics of modulation effect appearance - in the MC38 tumor the beneficial alterations in the landscape of TME were noted already 3 days after the administration of HES-MTX, whereas in B16 F0 tumors those changes occurred 10 days after the start of therapy.

The analysis of various MDSC subpopulations present in MC38 tumors revealed that HES-MTX affected the percentage of PMN-MDSCs, while the size of the M-MDSCs subpopulation remained unchanged. It is worth mentioning that among these two subpopulations, M-MDSCs show a more suppressive nature compared to PMN-MDSCs and may be an important immunosuppressor factor for T cell activity [34]. Considering this fact, the desired effect of therapy would be to reduce the size of the M-MDSC subpopulation [35]. However, the treatment with HES-MTX did not fulfill this criterium. This type of therapy resulted in temporary maintenance of the PMN-MDSC percentage on the low level, in contrast to MTX in free form. This effect was not prolonged and one week later in the HES-MTX group the percentage of these cells was significantly elevated. On the 3rd day of therapy, in MC38 nodules a decrease in the percentage of TAMs was observed. Moreover, this effect was long-lasting and was accompanied by high expression of MHC II on the surface of TAMs. Since such cells are reported as having a potent anti-tumor activity and inflammatory character [36-38], we suppose that these cells were involved in tumor growth inhibition. It should be highlighted that in MC38 tumors, TAMs constituted the most abundant immune cell type in comparison to both MDSC subpopulations. Thus, considering the TAMs' dominance in TME together with the high immunosuppressive features of part of these cells, we postulate that the immunomodulatory potential of HES-MTX was mainly concerned with the TAMs' population presented in MC38 tumors. All observed HES-MTX-induced alterations in the mentioned so far myeloid cells with potent immunosuppressive activity, were crucial in the increased influx of DCs into MC38 tumor tissue. Regardless of the fact that an elevated percentage of DCs in the tumor was observed only on the 3rd day of therapy, it should be underlined, that the beneficial modulatory effect of HES-MTX on the degree of activation status of those DCs persisted over time. It has been shown by others that certain cytostatics such as methotrexate or paclitaxel used in appropriate doses during DCs generation caused increased expression of costimulatory molecules and proteins associated with the processing of engulfed antigens, which additionally supports the activation level of those cells [4, 6]. Besides the mentioned research conducted in the *in vitro* assays, the results presented by us in the current study clearly confirm that HES-MTX showed a greater modulation potential than MTX in free form, even towards already differentiated DCs present in TME. Moreover, considering the influence of applied therapy on the size of lymphoid

cell subpopulations infiltrating the MC38 tumors, it was found that the main effect was visible shortly after HES-MTX administration and concerned temporary increase in the percentages of $CD8^+$ and NKT cells.

The above observations should be explained by the mutual relation of the size of individual immune cells subpopulations with opposite properties. The HES-MTX therapy resulted in an initial reduction in the size of the population of pro-tumor immune cells (TAMs and PMN-MDSCs), which enabled an increased influx of cells with strong anti-cancer activity (activated DCs, $CD8^+$ cells, NKT cells) into the MC38 tumor tissue.

However, in the B16 F0 tumor model, most of the changes indicating the immunomodulatory potential of HES-MTX, in this case, were observed long after the start of the therapy. These differences in the kinetics of immunomodulation occurrence should be related to the size of the MDSC population, which largely dominates the microenvironment of B16 F0 tumors. Considering a large number of these cells present in the tumor tissue, especially the M-MDSC population, it can be assumed that they are the main source of all suppressor factors that impair the formation and activation of cells with anti-tumor properties. Additionally, this observation may explain the delay in the occurrence of HES-MTX-dependent immunomodulation. In fact, it is well known that immunosuppressive cells, such MDSCs, TAMs and Tregs negatively affect the properties of $CD4^+$ and $CD8^+$ cells [39, 40], thereby constituting a major obstacle to the effective activation of an efficient anti-tumor response. Although treatment with HES-MTX resulted in a significant reduction in the percentage of TAMs and Tregs which were noted already on the 3rd day of therapy, due to the high proportion of M-MDSC in the B16 F0 tumors at that time, the beneficial influence of HES-MTX on the other immune cell subpopulations was abolished. The tumor progression-related two-fold reduction in the size of the M-MDSCs subpopulation which was observed on the 10th of therapy was sufficient to reveal the immunomodulatory potential of therapy with HES-MTX. Another important factor found at this time influencing the HES-MTX-induced changes in B16 F0's tumor landscape was the lowest percentage of PMN-MDSCs. All these mentioned alterations observed meanwhile were important to increase of the influx the $CD4^+$ cells and DCs into tumor tissue, but in the case of the latter subpopulation, it was not shown that the use of HES-MTX additionally affected the degree of activation of the cells.

On the basis of obtained results from the local and systemic anti-tumor immune response, it can be postulated that the changes within the tumor's lymphoid cell population, which occurred under the influence of HES-MTX administration, induced a similar effect at the level of the systemic immune response. Moreover, the kinetics of the appearance of the immunomodulation in the tumors was also reflected in the spleens. In the spleens obtained from MC38-tumor bearing mice, most of the HES-MTX-induced alterations were observed shortly after the administration of chemotherapeutic and included an increased percentage of $CD8^+$ and NKT cells, but only for the latter subpopulation this effect was long-lasting. Nevertheless, in the spleens harvested from B16 F0-tumor bearing mice, likewise the tumor tissue, the changes caused by the use of nanoconjugate were postponed in time and were limited to the increased percentages of $CD4^+$. In the case of systemic immune response, the immunomodulatory effect of HES-MTX was also manifested towards lymphoid cells, which were unaffected at the level of the local immune response. More precisely - in the MC38 tumor model, the percentage of splenic $CD4^+$ cells increased, whereas in the B16 F0 tumor model - the size of the splenic $CD8^+$ cell population enhanced. Furthermore, these changes occurred at a typical time point for each tumor model. All these findings suggest that, in both used tumor models, the immunomodulatory potential of HES-MTX affected the same populations of lymphoid cells, confirming our assumption that the changes induced at the local anti-tumor response level are also reflected in the cells in the spleen, considered to be the main site of the systemic anti-tumor response.

However, taking into consideration the direction of the immune response of splenocytes as a result of their secondary contact with tumor antigens, it should be underlined that between the two analyzed tumor models the differences in the type of immune response were noted. In the MC38-tumor model, restimulation of spleen cells resulted in the activation of a $CD8^+$-

dependent type of immune response. In turn, in the B16 F0 tumor model, the most abundant immune cell subpopulation among all restimulated splenocytes was constituted by NK cells. Regardless of the tumor model, the nanoconjugate elicited the initial enlargement in the percentage of $CD8^+$ cells after restimulation, while variations were evident at a later time point. Finally, treatment with HES-MTX resulted in an increase in the percentage of NK cells in the MC38 model, and $CD4^+$ cells in the B16 F0 model. And further differences resulting from the type of tumor model were evident in the ability of splenocytes to release cytolytic granules, which was also reflected in the capacity of spleen cells to specific elimination of tumor cells. In the MC38-tumor model, the greatest ability of restimulated spleen cells to degranulate and release the $CD107a^+$ molecules was observed in the case of $CD8^+$ and NK cells and occurred on the 3rd day of therapy with HES-MTX which corresponded with the increased cytotoxic activity of these splenocytes against MC38 cells. In the B16 F0 tumor model, the nanoconjugate-induced changes occurred on the 10th day of therapy and the increased expression of $CD107a^+$ granules concerned not only $CD8^+$ and NK cells but also $CD4^+$ cells. Similarly, all these changes were reflected in the increased cytotoxic activity of spleen cells obtained on the 10th day of therapy.

Summarizing, all these alterations again support our assumption about the immunomodulatory activity of HES-MTX in both tumor models, which, however, appears at different time points. This phenomenon may be closely related to the composition of the tumor microenvironment at the start of chemotherapy because the further progress of an effective immune response directed against the developing tumor depends on the presence and population size of cells with immunosuppressive properties. Moreover, the postponed modulation of the immune response, which was observed in the B16 F0 tumor model may also explain the greater difference in the therapeutic efficacy between MTX and HES-MTX-treated group of mice. The beneficial influence of HES-MTX on the immune response occurred later than in the case of MC38-bearing mice. This finally led to the enhanced, but shifted in time, anti-tumor activity of nanoconjugate in the B16 F0 tumor model. Whereas in the MC38 tumor model, the immunomodulatory potential of HES-MTX was slowly decreasing in time, which was also reflected in the smaller TGI value difference between both treated groups of mice.

Conclusion

The HES-MTX nanoconjugate shows immunomodulatory activity in both tested tumor models. However, this activity occurs at different time points, which may be due to differences in the composition of the tumor microenvironment and the rate of tumor growth. In the MC38 tumor model modulation of local and systemic immune response was noted already 3 days after the administration of HES-MTX, whereas in B16 F0 tumors those changes occurred 10 days after the start of therapy. The obtained results indicate the need for conscious choice of the next stages of treatment for a given type of cancer, especially in the case of immunotherapy, the effectiveness of which depends on the type of immune cells activated by the cancer.

Acknowledgements

This research was funded by National Science Centre, Poland (grant No. 2017/27/B/NZ6/02702).

Disclosure of conflict of interest

The authors declare that the research was conducted in the absence of any commercial or financial relationships that could be construed as a potential conflict of interest.

Address correspondence to: Agnieszka Szczygieł, Hirszfeld Institute of Immunology and Experimental Therapy, Polish Academy of Sciences, Wrocław, Poland. Tel: +48-71-3709928; E-mail: agnieszka.szczygiel@hirszfeld.pl

References

[1] Bailly C, Thuru X and Quesnel B. Combined cytotoxic chemotherapy and immunotherapy of cancer: modern times. NAR Cancer 2020; 2: zcaa002.

[2] Bracci L, Schiavoni G, Sistigu A and Belardelli F. Immune-based mechanisms of cytotoxic chemotherapy: implications for the design of novel and rationale-based combined treatments against cancer. Cell Death Differ 2014; 21: 15-25.

[3] Landreneau JP, Shurin MR, Agassandian MV, Keskinov AA, Ma Y and Shurin GV. Immunological mechanisms of low and ultra-low dose cancer chemotherapy. Cancer Microenviron 2015; 8: 57-64.
[4] Shurin GV, Tourkova IL, Kaneno R and Shurin MR. Chemotherapeutic agents in noncytotoxic concentrations increase antigen presentation by dendritic cells via an IL-12-dependent mechanism. J Immunol 2009; 183: 137-44.
[5] Kaneno R, Shurin GV, Tourkova IL and Shurin MR. Chemomodulation of human dendritic cell function by antineoplastic agents in low noncytotoxic concentrations. J Transl Med 2009; 7: 58.
[6] Kaneno R, Shurin GV, Kaneno FM, Naiditch H, Luo J and Shurin MR. Chemotherapeutic agents in low noncytotoxic concentrations increase immunogenicity of human colon cancer cells. Cell Oncol (Dordr) 2011; 34: 97-106.
[7] Shi GN, Hu M, Chen C, Fu J, Shao S, Zhou Y, Wu L and Zhang T. Methotrexate enhances antigen presentation and maturation of tumour antigen-loaded dendritic cells through NLRP3 inflammasome activation: a strategy for dendritic cell-based cancer vaccine. Ther Adv Med Oncol 2021; 13: 1758835920987056.
[8] Koźmiński P, Halik PK, Chesori R and Gniazdowska E. Overview of dual-acting drug methotrexate in different neurological diseases, autoimmune pathologies and cancers. Int J Mol Sci 2020; 21: 3483.
[9] Bol KF, Schreibelt G, Gerritsen WR, de Vries IJ and Figdor CG. Dendritic cell-based immunotherapy: state of the art and beyond. Clin Cancer Res 2016; 22: 1897-906.
[10] Wright NJ, Fedor JG, Zhang H, Jeong P, Suo Y, Yoo J, Hong J, Im W and Lee SY. Methotrexate recognition by the human reduced folate carrier SLC19A1. Nature 2022; 609: 1056-62.
[11] Visentin M, Zhao R and Goldman ID. The antifolates. Hematol Oncol Clin North Am 2012; 26: 629-48, ix.
[12] Nogueira E, Sárria MP, Azoia NG, Antunes E, Loureiro A, Guimarães D, Noro J, Rollett A, Guebitz G and Cavaco-Paulo A. Internalization of methotrexate conjugates by folate receptor-α. Biochemistry 2018; 57: 6780-6786.
[13] Javia A, Vanza J, Bardoliwala D, Ghosh S, Misra LA, Patel M and Thakkar H. Polymer-drug conjugates: design principles, emerging synthetic strategies and clinical overview. Int J Pharm 2022; 623: 121863.
[14] Hao F, Lee RJ, Yang C, Zhong L, Sun Y, Dong S, Cheng Z, Teng L, Meng Q, Lu J, Xie J and Teng L. Targeted co-delivery of siRNA and methotrexate for tumor therapy via mixed micelles. Pharmaceutics 2019; 11: 92.
[15] Li Y, He H, Jia X, Lu WL, Lou J and Wei Y. A dual-targeting nanocarrier based on poly(amidoamine) dendrimers conjugated with transferrin and tamoxifen for treating brain gliomas. Biomaterials 2012; 33: 3899-908.
[16] Thomas TP, Huang B, Choi SK, Silpe JE, Kotlyar A, Desai AM, Zong H, Gam J, Joice M and Baker JR Jr. Polyvalent dendrimer-methotrexate as a folate receptor-targeted cancer therapeutic. Mol Pharm 2012; 9: 2669-2676.
[17] Figueiró F, de Oliveira CP, Bergamin LS, Rockenbach L, Mendes FB, Jandrey EH, Moritz CE, Pettenuzzo LF, Sévigny J, Guterres SS, Pohlmann AR and Battastini AM. Methotrexate upregulates ecto-5'-nucleotidase/CD73 and reduces the frequency of T lymphocytes in the glioblastoma microenvironment. Purinergic Signal 2016; 12: 303-12.
[18] Brecher ME, Owen HG and Bandarenko N. Alternatives to albumin: starch replacement for plasma exchange. J Clin Apher 1997; 12: 146-53.
[19] Paleos CM, Sideratou Z and Tsiourvas D. Drug delivery systems based on hydroxyethyl starch. Bioconjug Chem 2017; 28: 1611-24.
[20] Xiao C, Hu H, Yang H, Li S, Zhou H, Ruan J, Zhu Y, Yang X and Li Z. Colloidal hydroxyethyl starch for tumor-targeted platinum delivery. Nanoscale Adv 2018; 1: 1002-1012.
[21] Wang H, Hu H, Yang H and Li Z. Hydroxyethyl starch based smart nanomedicine. RSC Adv 2021; 11: 3226-40.
[22] Xiao C, Li J, Wang X, Li S, Xu C, Zhang Z, Hua A, Ding ZY, Zhang BX, Yang X and Li Z. Hydroxyethyl starch stabilized copper-diethyldithiocarbamate nanocrystals for cancer therapy. J Control Release 2023; 356: 288-305.
[23] Goszczyński TM, Filip-Psurska B, Kempińska K, Wietrzyk J and Boratyński J. Hydroxyethyl starch as an effective methotrexate carrier in anticancer therapy. Pharmacol Res Perspect 2014; 2: e00047.
[24] Wilhelm S, Tavares AJ, Dai Q, Ohta S, Audet J, Dvorak HF and Chan WCW. Analysis of nanoparticle delivery to tumours. Nat Rev Mater 2016; 1: 1-12.
[25] Golombek SK, May JN, Theek B, Appold L, Drude N, Kiessling F and Lammers T. Tumor targeting via EPR: strategies to enhance patient responses. Adv Drug Deliv Rev 2018; 130: 17-38.
[26] Zein R, Sharrouf W and Selting K. Physical properties of nanoparticles that result in improved cancer targeting. J Oncol 2020; 2020: 5194780.
[27] Szczygieł A, Anger-Góra N, Węgierek-Ciura K, Mierzejewska J, Rossowska J, Goszczyński TM, Świtalska M and Pajtasz-Piasecka E. Immunomodulatory potential of anticancer therapy

composed of methotrexate nanoconjugate and dendritic cell-based vaccines in murine colon carcinoma. Oncol Rep 2021; 45: 945-962.
[28] Pajtasz-Piasecka E, Szyda A, Rossowska J, Krawczenko A, Indrová M, Grabarczyk P, Wysocki P, Mackiewicz A and Duś D. Loss of tumorigenicity of murine colon carcinoma MC38/0 cell line after transduction with a retroviral vector carrying murine IL-12 genes. Folia Biol (Praha) 2004; 50: 7-14.
[29] Pajtasz-Piasecka E, Rossowska J, Szyda A, Krawczenko A and Dus D. Generation of antitumor response by JAWS II mouse dendritic cells transduced with murine interleukin 12 genes. Oncol Rep 2007; 17: 1249-57.
[30] Rossowska J, Pajtasz-Piasecka E, Szyda A, Krawczenko A, Zietara N and Dus D. Tumour antigen-loaded mouse dendritic cells maturing in the presence of inflammatory cytokines are potent activators of immune response in vitro but not in vivo. Oncol Rep 2009; 21: 1539-49.
[31] Szczygieł A, Węgierek-Ciura K, Wróblewska A, Mierzejewska J, Rossowska J, Szermer-Olearnik B, Świtalska M, Anger-Góra N, Goszczyński TM and Pajtasz-Piasecka E. Combined therapy with methotrexate nanoconjugate and dendritic cells with downregulated IL-10R expression modulates the tumor microenvironment and enhances the systemic antitumor immune response in MC38 murine colon carcinoma. Front Immunol 2023; 14: 1155377.
[32] Ciekot J, Psurski M, Jurec K and Boratyński J. Hydroxyethylcellulose as a methotrexate carrier in anticancer therapy. Invest New Drugs 2021; 39: 15-23.
[33] Woźniak M, Pastuch-Gawołek G, Makuch S, Wiśniewski J, Krenács T, Hamar P, Gamian A, Szeja W, Szkudlarek D, Krawczyk M and Agrawal S. In vitro and in vivo efficacy of a novel glucose-methotrexate conjugate in targeted cancer treatment. Int J Mol Sci 2021; 22: 1748.
[34] Haverkamp JM, Smith AM, Weinlich R, Dillon CP, Qualls JE, Neale G, Koss B, Kim Y, Bronte V, Herold MJ, Green DR, Opferman JT and Murray PJ. Myeloid-derived suppressor activity is mediated by monocytic lineages maintained by continuous inhibition of extrinsic and intrinsic death pathways. Immunity 2014; 41: 947-59.
[35] Yaseen MM, Abuharfeil NM, Darmani H and Daoud A. Mechanisms of immune suppression by myeloid-derived suppressor cells: the role of interleukin-10 as a key immunoregulatory cytokine. Open Biol 2020; 10: 200111.
[36] Wang B, Li Q, Qin L, Zhao S, Wang J and Chen X. Transition of tumor-associated macrophages from MHC class II(hi) to MHC class II(low) mediates tumor progression in mice. BMC Immunol 2011; 12: 43.
[37] Movahedi K, Laoui D, Gysemans C, Baeten M, Stangé G, Van den Bossche J, Mack M, Pipeleers D, In't Veld P, De Baetselier P and Van Ginderachter JA. Different tumor microenvironments contain functionally distinct subsets of macrophages derived from Ly6C(high) monocytes. Cancer Res 2010; 70: 5728-39.
[38] Laoui D, Van Overmeire E, Di Conza G, Aldeni C, Keirsse J, Morias Y, Movahedi K, Houbracken I, Schouppe E, Elkrim Y, Karroum O, Jordan B, Carmeliet P, Gysemans C, De Baetselier P, Mazzone M and Van Ginderachter JA. Tumor hypoxia does not drive differentiation of tumor-associated macrophages but rather fine-tunes the M2-like macrophage population. Cancer Res 2014; 74: 24-30.
[39] Wu Y, Yi M, Niu M, Mei Q and Wu K. Myeloid-derived suppressor cells: an emerging target for anticancer immunotherapy. Mol Cancer 2022; 21: 184.
[40] Cook KW, Xue W, Symonds P, Daniels I, Gijon M, Boocock D, Coveney C, Miles AK, Shah S, Atabani S, Choudhury RH, Vaghela P, Weston D, Metheringham RL, Brentville VA and Durrant LG. Homocitrullination of lysine residues mediated by myeloid-derived suppressor cells in the tumor environment is a target for cancer immunotherapy. J Immunother Cancer 2021; 9: e001910.